Available online at www.sciencedirect.com

ScienceDirect

Procedia Structural Integrity 38 (2022) 77–83

Structural Integrity Procedia

www.elsevier.com/locate/procedia

FATIGUE DESIGN 2021, 9th Edition of the International Conference on Fatigue Design

Correlation between quasistatic und fatigue properties of additively manufactured AlSi10Mg using Laser Powder Bed Fusion

Andreas Kempf[a]*, Julius Kruse[b], Mauro Madia[b], Kai Hilgenberg[b]

[a]*Volkswagen Aktiengesellschaft, Brieffach 14370, 38436 Wolfsburg, Deutschland*
[b]*Bundesanstalt für Materialforschung und –prüfung (BAM), Unter den Eichen 87, 12205 Berlin, Deutschland*

Abstract

In order to find a resource efficient approach for the fatigue lifetime prediction of laser powder bed fusion (L-PBF) processed AlSi10Mg material, results of tensile and fatigue tests were compared. The specimens were manufactured with three different L-PBF machines and studied in different heat treatment conditions (as-built, annealed, T6 heat treated). The investigations showed that the high attainable tensile strength properties after the manufacturing process are not beneficial in the high cycle fatigue (HCF) regime. In contrast, the applied heat treatments, which lead typically to a decrease of ultimate tensile strength, improved dramatically the fatigue behavior. Additionally, a clear correlation between the elongation at fracture and HCF resistance has been found for individual heat treatment conditions. This empiric relationship provides an estimation of the fatigue resistance in the presence of material defects and can be implemented in part and process approvals.

Keywords: Additive Manufacturing; Laser powder bed fusion; AlSi10Mg; Tensile properties; Fatigue properties

1. Introduction

Qualification of additively manufactured (AM) components and processes is still challenging and requires an understanding of the relationship among technological parameters, microstructure, and resulting mechanical performance. For the perspective use of AM structures as safety-critical components, conventional approval processes need costly and time-consuming test series and are, thus, in contradiction with the high production flexibility achievable with those technologies. It is well known that the mechanical properties of parts produced with L-PBF –

* Corresponding author. Tel.: 05361-9-990523.
E-mail address: andreas.kempf1@volkswagen.de

10.1016/j.prostr.2022.03.009

one of the most prominent technology used for metal part AM – strongly depends on the microstructure. Large variations in the ultimate tensile strength (UTS) and yield strength of the aluminium alloy AlSi10Mg processed with different L-PBF machines have been found which showed a correlation to the size of the sub-cellular microstructure of separated Si particles (Kempf et al., 2020). In another study it was identified that such differences in tensile strength properties can be eliminated by post process heat treatments due to a homogenization in microstructure. Nevertheless, noticeable differences in the elongation at fracture remained caused by the presence of material defects (Kempf et al., 2021). Since the fatigue properties of L-PBF fabricated materials are also dominated by material imperfections (Blinn et al., 2020; Esmaeilizadeh et al., 2021; Romano et al., 2018; Masuo et al., 2018), the aim of this paper was to analyze the correlations between tensile and fatigue properties of AlSi10Mg material.

2. Experimental set-up

The different types of L-PBF systems used for specimen fabrication are given in Table 1 including the particle size distribution of the powders, the process parameters, and the build-up strategies. All specimens were orientated in z-direction (build direction). To avoid fluctuations of the manufacturing process in the interpretation of the results, tensile and fatigue specimens from each L-PBF machine were manufactured in the same building job. For tensile testing, rod specimens with a diameter of 11 mm and height of 80 mm were fabricated and then machined according to DIN 50125 standard geometry B6x30 (see Fig. 1a). Fatigue specimens were machined from rods, 16 mm in diameter and 110 mm in height, according to the geometry shown in Fig. 1b.

Table 1. Characterization of AlSi10Mg powders, process parameters, and build-up strategies used for specimen fabrication.

	Machine A	Machine B	Machine C
Machine type	SLM 280 HL	SLM 500	Concept Laser XLine 2000 R
Particle size of powder D_{10}, D_{50}, D_{90} in µm	24, 38, 60	27, 39, 54	41, 56, 71
Laser power P in W	700	350	950
Scanning speed v in mm/s	2260	1650	2450
Layer thickness d in µm	50	30	60
Hatch distance y in µm	170	130	180
Temperature of building platform in °C	150	150	200
Build-up strategy	Stripes (10 mm), 67° alternating	Stripes (10 mm) 67° alternating	Stripes (10 mm) 90° alternating

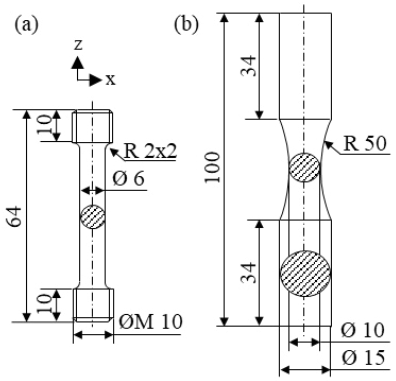

Fig. 1. Specimens' geometry; (a) tensile test; (b) rotating bending test.

Table 2. Experimental design for mechanical testing.

Test	Heat treatment	Machine A	Machine B	Machine C
Tensile test	As-built	X	X[1]	X[1]
	Annealed	X	X[1]	X[1]
	T6	X	X[1]	X[1]
Fatigue test	As-built	X	X	X
	Annealed			X
	T6	X	X	X

[1]Tests were performed in (Kempf et al., 2021).

Tensile tests were performed according to DIN EN ISO 6892-1 standard at room temperature with a strain rate of 0.006 s^{-1}. Five specimens per batch were tested with a Zwick Z250 SW universal standard machine. Wöhler (S-N) curves were determined on a Walter + Bai rotating bending testing machine (R = -1). Fatigue tests were conducted according to DIN 50113 at room temperature up to a maximum of 10^7 cycles applying a testing frequency of 60 Hz. The stress amplitude for the hour-glass type fatigue specimens were established regarding the fracture origin. Tensile and fatigue properties were detected in the as-built condition, after an annealing heat treatment (300 °C/ 2 h), as well as after a T6 heat treatment (525 °C/ 2 h – water quenching – 160 °C/ 8h). The experimental design is reported in Table 2.

Fractographic investigations were carried out on fatigue specimens. Therefore, a scanning electron microscope (SEM) Tescan Mira XMU with a secondary electron detector working at a voltage of 15 kV was applied.

3. Tensile properties

Table 3 summarizes the mechanical properties obtained from tensile testing. Herein, results from preliminary studies are included so that only the most important facts are reported in this section. Detailed discussions of the interactions between microstructure and resulting quasistatic properties can be found in (Kempf et al., 2020; Kempf et al., 2021).

The as-built properties reveal slightly higher standard deviations than the heat treated specimens. Nevertheless, the determined standard deviations are negligibly small for all batches so that they do not have to be taken into account in data interpretation. The as-built conditions of the different L-PBF machines show significant differences in the quasistatic strength properties. Ultimate tensile and yield strength vary between 346-484 MPa and 228-292 MPa, respectively. These deviations were leveled out almost completely for both heat treatments. Thereby, the annealed specimens exhibit considerably decreased values in ultimate tensile and yield strength which are in range between 265-272 MPa and 142-162 MPa, respectively. The T6 heat treatment also reduces the ultimate tensile strength for all

Table 3. Mean values and standard deviations of tensile properties of different L-PBF machines in different heat treatment conditions.

Characteristic	Heat treatment	Machine A	Machine B	Machine C
Ultimate tensile strength UTS in MPa	As-built	418 ± 12	484 ± 8[1]	346 ± 14[1]
	Annealed	268 ± 1	272 ± 2[1]	265 ± 1[1]
	T6	311 ± 1	302 ± 2[1]	304 ± 4[1]
Yield strength YS in MPa	As-built	263 ± 5	292 ± 2[1]	228 ± 9[1]
	Annealed	143 ± 1	162 ± 3[1]	142 ± 1[1]
	T6	247 ± 1	242 ± 2[1]	248 ± 2[1]
Elongation at fracture A in %	As-built	3.0 ± 0.3	4.8 ± 0.6[1]	1.7 ± 0.3[1]
	Annealed	9.8 ± 0.5	12.4 ± 0.4[1]	5.3 ± 0.5[1]
	T6	7.5 ± 0.4	9.6 ± 0.4[1]	4.2 ± 0.4[1]

[1]Results according to (Kempf et al., 2021).

L-PBF machines to 302-311 MPa, but an increase in the yield strength (242-248 MPa) can be reached by this procedure. The ductility is dramatically improved with both heat treatments. The annealing heat treatment resulted in slightly higher values in the elongation at fracture than the T6 heat treatment. However, ductility of specimens of the three L-PBF machines were not homogeneous. For each heat treatment condition, specimens of L-PBF machine B exhibit the highest elongation at fracture, whereas L-PBF machine C produces the lowest ductility values.

4. Fatigue properties

A comparison of the fatigue properties in different heat treatment conditions – examined at specimens manufactured with L-PBF machine C – is illustrated in Fig. 2 showing an increased HCF resistance for heat treated specimens. Similar results have been found by other researchers who explained these observations by the increased elongation at fracture. König et al. see a reduced notch sensitivity in the higher ductility so that stress concentration at material defects can be decreased by plastic flowing (König et al., 2020). Buchbinder relates the higher fatigue strength to the higher crack propagation resistance of a nucleated crack in the coarsened microstructure in heat treated specimens (Buchbinder, 2013). However, since the elongation at fracture and the HCF resistance show a contrary trend for the annealing and T6 heat treatment, a relationship between these mechanical properties cannot be identified

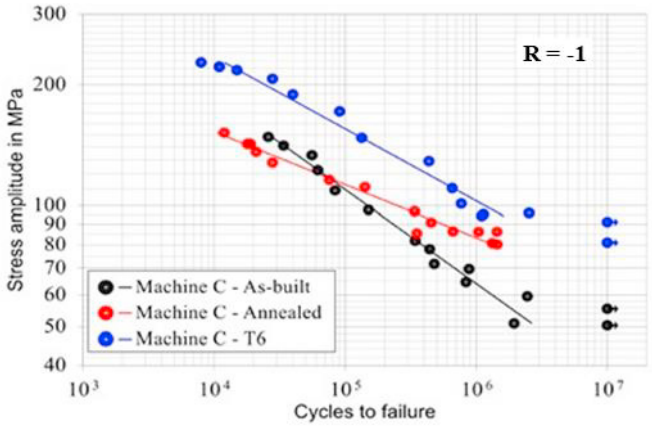

Fig. 2. S-N-curves in the as-built, annealed, and T6 heat treated condition of specimens manufactured with L-PBF machines C.

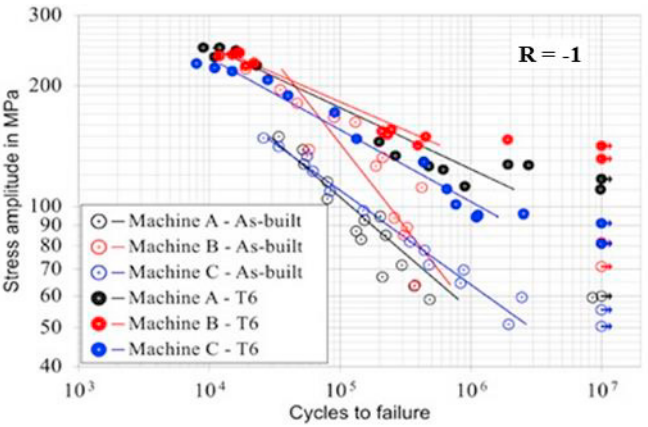

Fig. 3. S-N-curves in the as-built and T6 heat treated condition of specimens manufactured with the three different L-PBF machines.

for different heat treatment conditions of L-PBF processed AlSi10Mg. A possible explanation can be found in the different microstructure. It was found that the T6 heat treatment coarsens the initial sub-cellular microstructure even more than the annealing heat treatment (Kempf et al., 2021). Nevertheless, the elongation at fracture in the T6 condition is lower which can be traced back to precipitated Mg_2Si phase which has a detrimental impact on the ductility properties.

Fig. 3 shows the S-N curves in the as-built and T6 condition for the three L-PBF machines. In accordance with the results of L-PBF machine C, the fatigue performance of specimens manufactured with L-PBF machine A and B is increased after the T6 heat treatment. In general, the raise in HCF resistance caused by this heat treatment is in the order of 75% to 95%. Similar to the values in the elongation at fracture, there are noticeable differences in the HCF strength properties between the three L-PBF machines – in both heat treatment conditions. To explain this result, fractographic analyses of the fracture surfaces were conducted which will be present in the next section. Since the deviations in the HCF resistance between the three L-PBF machines do not vary significantly in both heat treatment condition, fracture surfaces were only examined at T6 heat treated specimens.

5. Fractographic analysis

All fracture surfaces of the T6 heat treated rotating bending test specimens were analyzed regarding the origin of the fracture. The examinations revealed that cracks were initiated at defects at or near the surface. Hereby, most of the cracks started at lack of fusion defects. Only one specimen failed due to the presence of regular shaped keyhole pores. Examples for these different, crack initiating defects are illustrated in Fig. 4.

The identified defects were evaluated statistically. In a first step, the quantity of specimens was determined which failed due to a singular and multiple crack initiation, respectively. Furthermore, the number of crack initiating defects

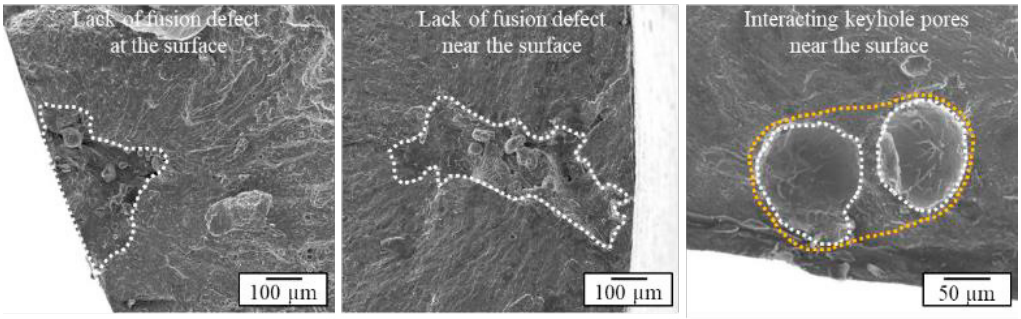

Fig. 4. Kinds of observed defects leading to crack initiation.

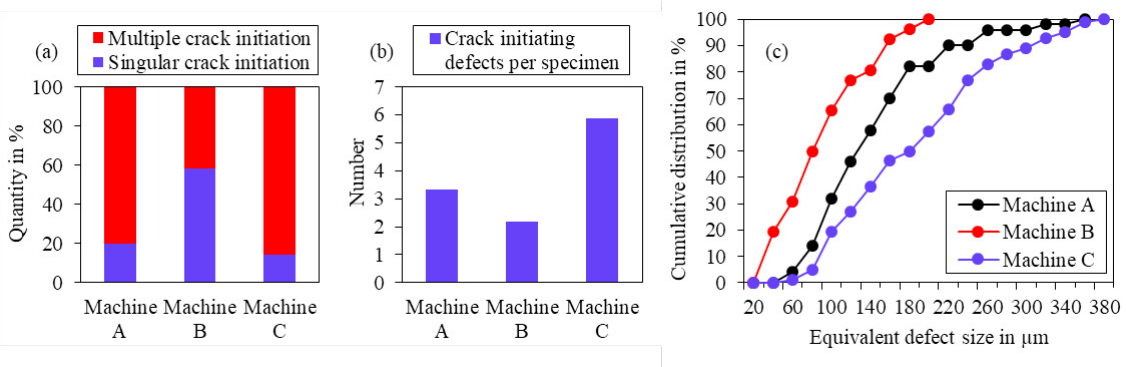

Fig. 5. Statistical evaluation of crack initiating defects; (a) singular vs. multiple crack initiation; (b) number of crack initiating defects per specimen; (c) cumulative defect size distribution; Specimens were manufactured with the three different L-PBF machines and analysed in the T6 heat treatment condition.

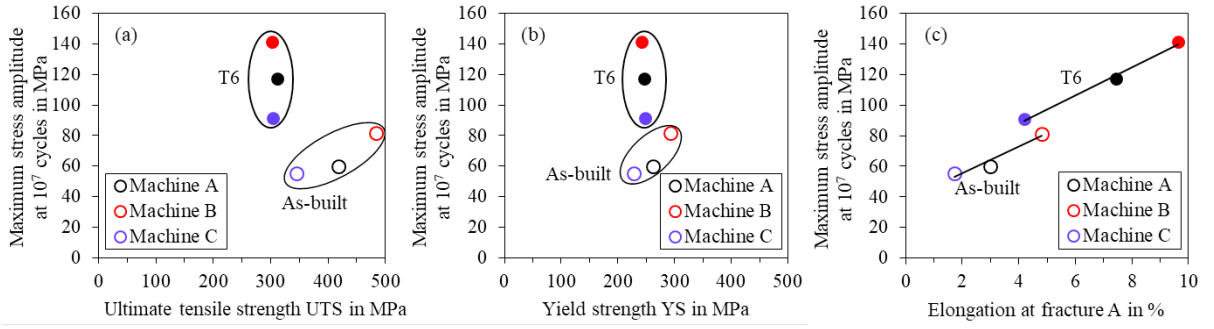

Fig. 6. Comparison of tensile and fatigue properties; (a) ultimate tensile strength vs. maximum stress amplitude at 10^7 cycles; (b) yield strength vs. maximum stress amplitude at 10^7 cycles; (c) elongation at fracture vs. maximum stress amplitude at 10^7 cycles; Values of specimens manufactured with the three different L-PBF machines in the as-built and T6 heat treatment condition.

per specimen was determined. Defects in L-PBF processed materials are usually distributed 'regularly' in the overall part volume. Hence, these analyses allow a comparative evaluation regarding the porosity between the specimens fabricated with the different L-PBF machines, since the presence of defects in the stress-critical surface area of the mechanically finished rotating bending test specimens becomes increasingly likely with an increasing porosity. The results are summarized in Fig. 5a and b emphasizing the lowest porosity for specimens processed with L-PBF machine B. Nearly 60% of these specimens failed due to a singular defect. The number of crack initiating defects per specimen is in the order of 2. In contrast, the manufacturing process with L-PBF machine C led to the highest porosity. Only 14% of the specimen showed a singular crack initiation. The number of crack initiating defects per specimen reaches a value of about 6. Additionally, the size of each defect was measured and the equivalent defect diameter was calculated. The cumulative defect size distribution in Fig. 5c highlights that specimens of L-PBF machine B contain the smallest defects, whereas those fabricated with L-PBF machine C the largest ones. Based on these results, the observed differences in the HCF performance between the three L-PBF machines become plausible.

6. Correlation of tensile and fatigue properties

To estimate the fatigue strength of metal parts, empirical relationships with quasistatic strength properties from tensile tests can be found in literature. For aluminium alloys, the fatigue strength is in the order of 0.25 UTS to 0.35 UTS (Issler et al., 1997). That is valid up to an ultimate tensile strength of 325 MPa. A further increase in the ultimate tensile strength does not improve the HCF resistance (König et al., 2020). The ultimate tensile strength in the as-built condition of specimens processed with the three L-PBF machines are in range between 346 to 484 MPa so that the HCF lifetime should not differ. Interestingly, a comparison with the maximum stress amplitude of fatigue specimens who passed 10^7 cycles reveals an improvement of the HCF resistance with increasing ultimate strength (Fig. 6a). However, this apparent contradiction can be explained by the size of the pre-existing material defects which has been demonstrated in the section before. Furthermore, a connection between ultimate tensile strength and HCF resistance is refuted, if the T6 heat treated specimens are included in the discussion. On the one hand, the ultimate tensile strength of these specimens is lower than those in the as-built condition, but the heat treatment improves dramatically the HCF strength. On the other hand, the T6 heat treatment promotes a homogenization in the microstructure so that differences in ultimate tensile strength between the three L-PBF machines were removed. Nevertheless, due to the impact of the material defects, differences in the HCF resistance were obtained. Finally, these are also the reasons why the yield strength does not correlate with the fatigue properties (Fig. 6b).

As already discussed in section 4, a general relationship between ductility and HCF properties seems not to be valid for L-PBF processed AlSi10Mg if different heat treatment conditions are considered. However, as depicted in Fig. 6c, the elongation at fracture correlates very well with the HCF resistance for the individual examined heat treatments. Fracture surface analyses in Fig. 5 revealed that an increasing defects size (which reduces the HCF strength) is accompanied with an increasing number of defects which causes an increased porosity and, thus, a decreased elongation a fracture. This can be seen as a possible verification of the observed relationship between the 'global'

depended elongation at fracture and the 'local' affected HCF resistance – in case of the presence of predominant existing lack of fusion defects.

7. Conclusion

Within this study, tensile and fatigue properties of L-PBF processed AlSi10Mg materials were determined including three different L-PBF machines and three different heat treatment conditions (as-built, 300 °C/ 2 h, T6). The following major conclusions have been found:

- As-built specimens show the highest quasistatic strength properties, but also the lowest ductility. Differences in the quasistatic strength obtained from the different L-PBF systems can be leveled out by the applied heat treatments accompanied with a reduction in the ultimate tensile strength and an increase in the elongation at fracture. Nevertheless, differences in the elongation at fracture between specimens manufactured with different L-PBF machines are still remaining.
- Fatigue properties in the as-built condition are much lower than after heat treating. The T6 heat treatment increases the HCF resistance even more than the annealing procedure. The HCF performance of specimens manufactured with the different L-PBF machines shows significant differences in the as-built as well as in the T6 heat treated condition.
- In contrast to the tensile strength properties, a correlation between the elongation at fracture and HCF resistance has been found for individual heat treatment conditions caused by the presence of predominant existing lack of fusion defects. This empirical relationship provides a cost- und time-reducing approach to
    - evaluate L-PBF machine manufacturers and suppliers of L-PBF components
    - prove the part quality achieved with a L-PBF machine
    - approve L-PBF manufactured components and the L-PBF process
    - achieve a high production flexibility (parts from different L-PBF machines)

References

Blinn, B., Krebs, F., Ley, M., Teutsch, R., Beck, T., 2020. Determination of the influence of a stress-relief heat treatment and additively manufactured surface on the fatigue behavior of selectively laser melted AISI 316L using efficient short-time procedures. International Journal of Fatigue 131, 105301.

Buchbinder, D., 2013. Selective Laser Melting von Aluminiumgusslegierungen. Shaker Verlag, Aachen.

Esmaeilizadeh, R., Keshavarzkermani, A., Ali, U., Behravesh, B., Bonakdar, A., Jahed, H., Toyserkani, E., 2021. On the effect of laser powder-bed fusion process parameters on the quasi-static and fatigue behaviour of Hastelloy X: A microstructure/defect interaction study. Additive Manufacturing 38, 101805.

Issler, L., Ruoß, H., Häfele, P., 1997. Festigkeitslehre – Grundlagen, 2nd Edition, Springer Verlag, Berlin Heidelberg.

Kempf, A., Hilgenberg, K., 2020. Influence of sub-cell structure on the mechanical properties of AlSi10Mg manufactured by laser powder bed fusion. Material Science & Engineering A 776, 138976.

Kempf, A., Hilgenberg, K., 2021. Influence of heat treatments on AlSi10Mg specimens manufactured with different laser powder fusion machines. Material Science & Engineering A 818, 141371.

König, K., Görres, F., Lübbecke, S., Löwisch, G., Brenner, S., Nedeljkovic-Groha, V., 2020. Failure of additively manufactured specimens of AlSi10Mg under cyclic loading, 5. Tagung des DVM-Arbeitskreises Additiv gefertigte Bauteile und Strukturen. Berichtsband 405, 41-54.

Masuo, H., Tanaka, Y., Morokoshi, S., Yagura, H., Uchida, T., Yamamoto, Y., Murakami, Y., 2018. Influence of defects, surface roughness and HIP on the fatigue strength of Ti-6Al-4V manufactured by additive manufacturing. International Journal of Fatigue 117, 163-179.

Romano, S., Brückner-Foit, A., Brandão, A., Gumpinger, J., Ghidini, T., Beretta, S., 2018. Fatigue properties of AlSi10Mg obtained by additive manufacturing: Defect-based modelling and prediction of fatigue strength. Engineering Fracture Mechanics 187, 165-189.